MICHIGAN STATE UNIVERSITY

CYCLOTRON LABORATORY

NUCLEAR COLLISIONS AT INTERMEDIATE ENERGIES

LECTURES PRESENTED AT THE
INTERNATIONAL SCHOOL ON NUCLEAR PHYSICS,
ALUSHTA, CRIMEA, USSR, 14-25 APRIL 1980

D. K. SCOTT

MARCH 1980

MSUCL-326

MSUCL-326
June 1980

NUCLEAR COLLISIONS AT INTERMEDIATE ENERGIES

D.K. Scott
National Superconducting Cyclotron Laboratory
Michigan State University
East Lansing, Michigan 48824

and

Département de Physique Nucléaire
C.E.N. Saclay
BP. No2, 91190 Gif-sur-Yvette

Introduction

The study of heavy ion reactions at intermediate energies, which we loosely define between 10 and 200 MeV per nucleon, has for sometime been recognized as important for providing links between low energy concepts and the superficially different approaches of relativistic heavy ion collisions. In this energy region, the average excitation increases beyond the characteristic intrinsic particle energies (≈30 MeV), with a concommittant diminution of the importance of quantal effects and an increased relevance of classical behaviour. Instead of a mean field description, one may find that the mean free path becomes short before nuclei lose their cohesiveness; hydrodynamic features may then come into play. From the perspective of general physics, the field of intermediate energy collisions is likely to be very interesting. One is neither in a quantal or a classical situation, neither in the one-body nor the two body extreme, neither close to the adiabatic nor the sudden regime. The explanation of phenomena in this region may therefore require the development of new theoretical approaches.

Through historical accident, the evolution of accelerators over the last decade has bypassed this interesting energy region. As indicated[/1/] in Fig. 1.1,[†] many accelerators exist around the world with energies up to 10 MeV/nucleon. In the early seventies, speculations about new states of matter at high densities spurred the development of high energy heavy ion beams on

[†]For clarity some of the illustrations in this paper have been redrawn from the originals. Reference should be made to the original literature for precise quantities.

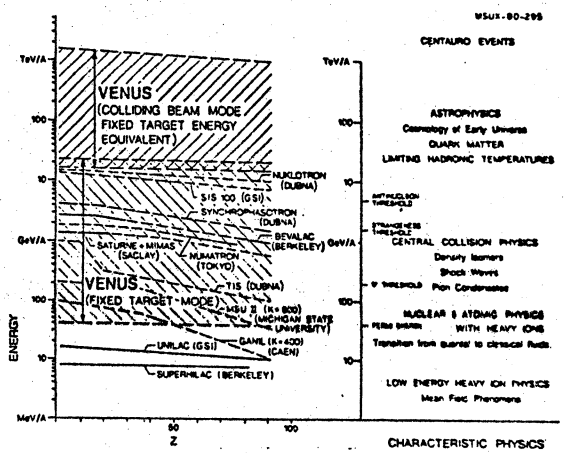

FIG. 1.1

existing synchrotrons at the Berkeley Bevalac, the Dubna Synchrophasotron, and Saturne II at Saclay, all of which reach to GeV/nucleon energies. The evidence for the highlights of the characteristic physics shown at the right is no longer entirely negative. There are indications for hydrodynamical[/2,3/] and shock wave effects,[/4,5/] for phase transitions,[/5,6/] limiting hadronic temperatures[/7/] and possibly forms of quark matter.[/8/] To pursue these hints with greater power and to study the physics of this regime, a new generation of high energy accelerators is under construction in many countries. These include accelerators specifically designed to cover the virgin territory of the intermediate energy region, such as the projects at Michigan State and Caen. The boldest proposal of the Venus Accelerator at Berkeley[/1/] recognises the importance of launching an attack on a broad energy front from 40 MeV/nucleon up to 1 TeV/nucleon, where the "mythical" Centauro events may become accessible in the laboratory.[/9/]

Existing low and high energy accelerators have been pushed to their limits for an initial exploration of the intermediate energy domain. These lectures will be concerned with the extent to which the results show a promise of reaping the expected rich harvest. The first lecture presents a general framework for discussing heavy ion reactions over a wide region of incident energies in terms of the participant - spectator model. The subsequent two lectures deal with the foundations of, and some deviations from, this simple picture. It is within these deviations that the onset of exotic new phenomena must be sought in intermediate energy collisions.

1. The Participant - Spectator Path

The outcome of nuclear collisions at relativistic energies differs from our low energy experience. Instead of the dominant two body final states it frequently happens that projectile and target are completely disintegrated into the constituent nucleons. However such explosive events may already appear at low energies. Fig. 1.2 shows a collision of Ne on Ne at 27 MeV/nucleon, taken in a streamer chamber, in which nine charged particle tracks emerge.[10] To give some conceptual understanding of these events at high energies the participant - spectator model, illustrated[11] in Fig. 1.3, was proposed. After the collision, the non-overlapping parts of the beam and target nuclei, called the spectators, continue along straight line trajectories. In the overlap region, strong interactions between the nucleons cause fragments to be emitted over a wide angular range. These participants constitute the nuclear fireball, which moves with a velocity intermediate between those of the target and projectile spectators.

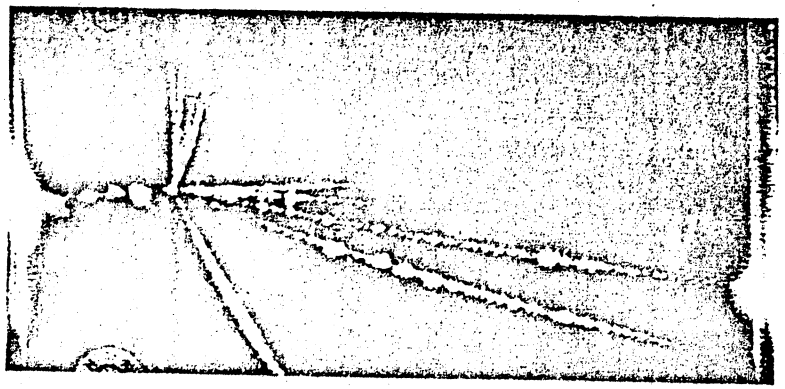

FIG. 1.2

The spectators and participants can be isolated by means of the rapidity plot, shown on the right of Fig. 1.3. Contours of invariant cross section are displayed in the plane of $p_{||}/mc$ and $p_{\perp}/mc$ which non relativistically measure the velocities parallel to and perpendicular to the beam direction. Concentric contours emanating from a point on the x-axis serve to identify the source of emission.

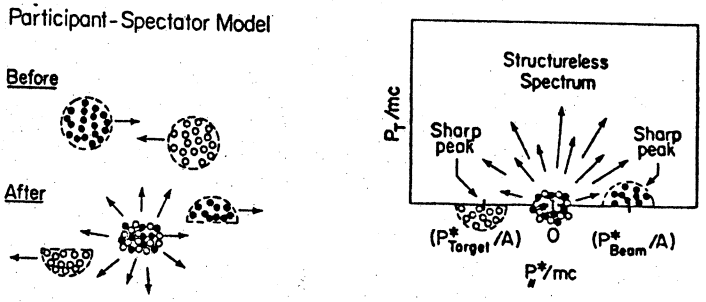

FIG. 1.3

Although this geometrical model represents an over-simplified view of the complexity of a relativistic nuclear collision, the basic elements are still discernable in more sophisticated theories, like the cascade and hydrodynamics.[2] The density, temperature and velocity profiles, generated in the hydrodynamical description of Ne + U at 400 MeV/nucleon with an impact parameter of 6 fm (Fig. 1.4) clearly identify a high velocity, low density (fragmented) projectile remnant, a low velocity target spectator and an intermediate velocity zone of high temperature resembling the nuclear fireball. Experimentally this region can be highlighted by imposing on the rapidity plot the additional constraint that the high multiplicity of charged particles from the exploding fireball be registered in an array of tag counters.[12] In this way the high temperature spectra of protons and pions shown in Fig. 1.5 are produced. For the moment, we simply note that these energy spectra have an exponential high energy behaviour, $\exp(-E/T)$, from which a fireball temperature is deduced, and we ignore the difference between p and π slopes, as well as the theoretical curves of a more sophisticated blast wave model.[13]

Such temperatures have been extracted for a variety of colliding systems from energies of 200 MeV/nucleon up to the highest available of 3.6 GeV/nucleon at the Dubna Synchrophasotron (see Fig. 1.1), and they are plotted[7] as a function of incident energy in Fig. 1.6. Here the vertical bars do not represent errors, but the range of temperatures deduced for different initial systems and different final state particles; one characteristic system is indicated. These differences are intriguing per se, and may be evidence for collective and hydrodynamical effects, but our present interest is rather in the overall smooth trend, which approaches a temperature of 140 MeV, the "boiling point of hadronic matter". This limiting temperature exists in the case of an exponential growth of particles which, by their creation, prevent further increase of random kinetic

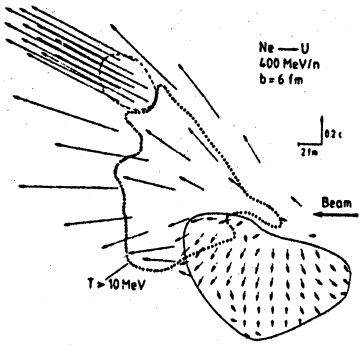

FIG. 1.4

energy in the fireball.[14] The clear existence of this limit must await future experiments on higher energy accelerators, and we turn our attention to the trend of the curve in the lower energy regime.

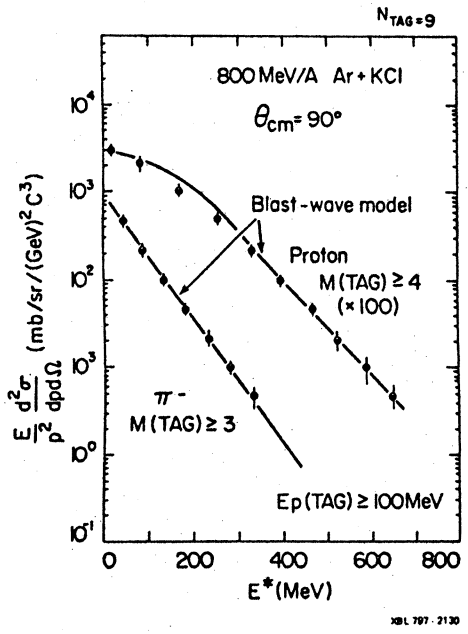

FIG.1.5

As the incident energy is reduced the fireball becomes less well separated in velocity from the spectators, and could eventually be trapped for the duration of the collision between the surrounding nuclei. In this spirit the logical extrapolation of the fireball is the hot-spot (see Fig. 1.6). The formal basis for the existence of hot-spots in nuclei will be deferred until the next section; it relies on a knowledge of the temperature dependence of the mean free path and thermal conductivity of nuclear matter. From an experimental viewpoint there is now a substantial body of evidence to suggest that such objects exist.

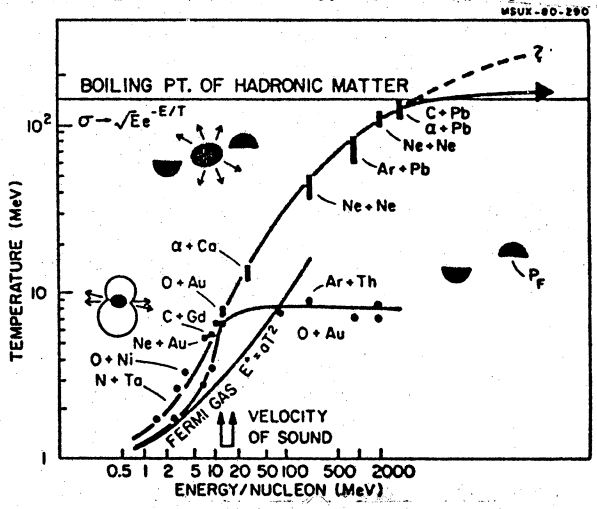

FIG. 1.6

One experimental result is shown in Fig. 1.7 for the proton spectra emitted in collisions of ^{16}O on ^{197}Au at an incident energy close to 20 MeV/nucleon.[15] These spectra are quite analagous to the fireball spectra[16] of Fig. 1.5 (except that there is no high multiplicity selection imposed - see the next section) and indeed exhibit rather similar features. It is quite clear that they cannot originate from a classical compound nucleus. By extending up to energies of 80 MeV with substantial cross-section, they require temperatures much too high: the center of mass energy of 200 MeV above the barrier leads to T = 2.9 MeV for the compound system, using $E^* = \frac{A}{8}T^2$, and we expect a decrease of 10^9 in cross section between 10 and 70 MeV, compared to the observed factor of only 10^3. What type of source, one therefore asks, is responsible for this emission? To find

out we fit the data with the expression,

$$\sigma(\theta_L, E_L) = \sqrt{E_L}\ \sigma_{INV}\ e^{-(E_L - 2a\sqrt{E_L}\cos\theta_L + a^2)/T}$$

where T is the source temperature, and "a^2" is the energy of a proton with the velocity of the source. The best fits, shown by the full line in Fig. 1.7, correspond to a source velocity of 0.1 c in the laboratory at a temperature of 8.1 MeV. We identify these parameters with a hot-spot and plot the temperature on Fig. 1.6, the point for ^{16}O + Au at ≃ 15 MeV/nucleon, which is the energy above the barrier. (Our analysis is also obviously closely related to the fireball model, and indeed the results of such a calculation, using parameters strictly in accord with the high energy formulation, gives a reasonable account of the data - the dashed lines). These data must also find an explanation in a more microscopic preequilibrium model, which we discuss in the next lecture.

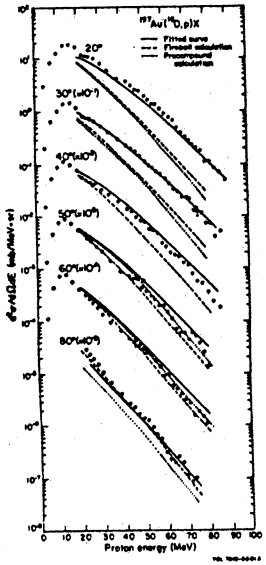

FIG. 1.7

Similar experiments[17] on alpha emission induced by Ne beams have recently been reported at energies of 290 and 400 MeV. (i.e. 14.5 and 20 MeV/nucleon) In the absence of a detailed analysis, we simply deduce the "hot-spot" temperatures from the 90° spectra (see earlier equation for $\sigma(\theta_L, E_L)$) and add them to Fig. 1.6. Also shown is a temperature of 6 MeV reported[18] for hot-spot formation in ^{12}C + ^{158}Gd at 152 MeV (i.e. 7.6 MeV/nucleon above the barrier). In perhaps the most sophisticated experiment, the asymmetries of energy spectra for α particles, detected[19] in coincidence with projectile fragments from reactions of ^{16}O on ^{58}Ni at 96 MeV, led to a hot-spot temperature of 3.5 MeV. Finally we note the lower energy studies[20] of α particles from ^{14}N + Ta in which an angle dependent temperature arises from the cooling of a hot-spot under rotation. We also interpret these data as examples of moving hot-spots at the temperatures shown in Fig. 1.6.

We now connect the hot-spot region to the fireball with a continuous line from 1 MeV/nucleon to 3.6 GeV/nucleon, adding data from a fireball analysis[21] of α + Ca at 25 MeV/nucleon as a bridging point. (In this presentation of data we have not included results from hot-spot analyses of proton induced reactions,[22,23] which in general lead to lower temperatures than α and heavy ion induced reactions). The smooth trend is taken as evidence in support of our assumed logical interpolation between the concept of a spatially localised hot-spot at low energy and the moving fireball at high energy. In order to pinpoint the transition we turn from the hot participants to the cold spectators.

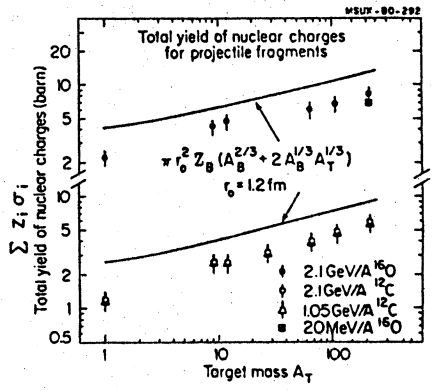

FIG. 1.8

When the fireball becomes separated as an identified flying object, the spectators should also be observed. For their identification, let us turn first to the geometrical implications of Fig. 1.3. The average number of participant protons which come from the beam nucleus, z_B^p, can be calculated as follows.[11] If a proton inside the projectile hits the target, it becomes a participant

proton, but otherwise it remains a spectator. If the nucleus consists of Z_B independent protons and N_B independent neutrons, then

$$\langle Z_B^P \rangle = Z_B \pi r_o^2 A_T^{2/3} / \sigma_{TOT} = Z_B A_T^{2/3} / (A_B^{1/3} + A_T^{1/3})^2$$

The total yield of protons carried in the projectile fragments is then,

$$Z_B - \langle Z_B^P \rangle \times \sigma_{TOT} = \pi r_o^2 Z_B (A_B^{2/3} + 2A_B^{1/3} A_T^{1/3}).$$

In Fig. 1.8, this prediction is compared with the yield of proton numbers from projectile fragments, deduced from the observed isotope yields in ^{16}O and ^{12}C induced reactions at 2.1 and 1.05 GeV/nucleon. The data points are obtained from $\Sigma \sigma_i Z_i$ where σ_i are the measured cross sections. Both the target mass dependence and the energy dependence are well reproduced by the simple participant-spectator model, and even the absolute magnitude is correct within 30%. Now we make the important observation that the yield of projectile charges for ^{16}O induced reactions[24] on ^{208}Pb at the much lower incident energy of 20 MeV/nucleon is almost identical to the yield at 2.1 GeV/nucleon. The surprising but logical conclusion is the validity of the participant-spectator model already at an energy of 20 MeV/nucleon

For additional proof, we look in more detail at the properties of spectators produced by the rapid abrasion process.[25] Suppose that the A nucleons of the projectile are assembled with zero net three momentum, $P_A = 0$. If F of these nucleons, chosen at random, are suddenly released as a single fragment, what would be the mean square total momentum P_F^2? The A nucleons have mean square momentum $\langle p^2 \rangle$, correlated by the requirement $P_A = 0$, so that,

$$A\langle p^2 \rangle + \sum_{i \neq j} \langle pi \cdot pj \rangle = 0$$

or

$$\langle\langle pi \cdot pj \rangle\rangle = -\langle p^2 \rangle / A-1.$$

where the double bracket denotes an average over all $i \neq j$. Then we get,

$$P_F^2 = \langle\langle (\sum_{i=1}^{F} p_i)^2 \rangle\rangle = \frac{F(A-F)}{(A-1)} \langle p^2 \rangle$$

and $\langle p^2 \rangle$ is just the mean square momentum associated with the Fermi motion of the nucleons, i.e. $3/5\ p_F^2$. Therefore a measurement of each Cartesian component of the momentum distribution of fragments released by the abrasion process will yield a gaussian distribution of the form $\exp(-p^2/2\sigma^2)$, where

$$\sigma^2 = \frac{P_F^2}{5} \frac{F(A-F)}{A-1} = \sigma_o^2 \frac{F(A-F)}{A-1} .$$

Striking verification comes from experiments with Argon at 213 MeV/nucleon.[26] The spectrum for a typical fragment ^{34}S is shown in Fig. 1.9, which is indeed a distribution of gaussian form, peaked at an energy corresponding closely to the fragment travelling with the velocity of the incident beam, as we expect for a spectator projectile fragment. In fact the velocity at the peak is slightly less (6850 MeV instead of 7240 MeV); some reduction is expected on account of the separation energy.[24] The values of σ_o deduced from a gaussian fit to the peak in momentum space, as well as to all the other observed fragments between Z=8 and 16, are shown at the bottom of the figure. The values are remarkably constant with a mean of σ_o = 94 MeV/c corresponding to P_F = 210 MeV/c, and quite close to the Fermi momentum[27] of 250 MeV c. The precise significance of the observed value is not yet fully understood.

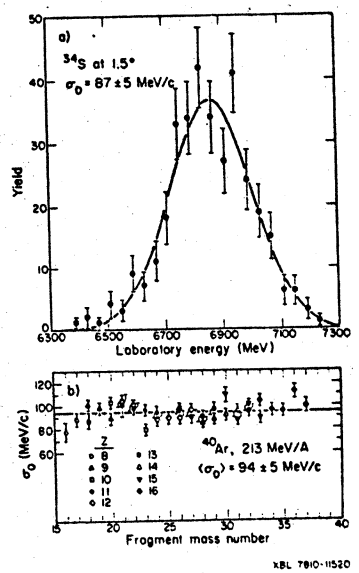

FIG. 1.9

This type of experiment has been repeated for other projectiles and over a very wide range of incident energies up to 2 GeV/nucleon. It has been possible[24,28] to identify projectile spectator fragments with the above properties down to energies of 20 MeV/nucleon; i.e. from 20 MeV/nucleon to 2 GeV/nucleon, the width of the momentum distribution is almost constant, characterised by a σ_o value in the region of 86 to 94 MeV/c. In order to display this constancy

in the temperature versus energy plot of Fig. 1.6, we transform the momentum width to an effective temperature by means of the relation,

$$\frac{3}{5}\frac{p_F^2}{2m} = 3\frac{\sigma_o^2}{2m} = \frac{3}{2}T$$

where m is the nucleon mass. The value of T associated with 86 MeV/c is then ≈8 MeV. The constancy of σ_o, reflected in the values of T, is clearly demonstrated in Fig. 1.6, down to 20 MeV/nucleon, below which the value suddenly decreases. Within the framework of the above discussion, this constancy of σ_o at a value closely reflecting the Fermi motion of the abraded fragments, cut loose from the parent projectile, is a demonstration of the validity of the spectator concept from energies of 20 MeV/nucleon upwards.

Although we introduced the parameter of temperature artifically in discussion of spectator fragments, it is interesting to note that a limiting value of 8 MeV is also expected for the thermodynamic production of complex fragments from a light nucleus. To see this we use the equation of state for a Fermi gas, $E^* = \frac{a}{8}T^2$, where "a" is the number of nucleons in the excited region with excitation energy E^*. If this excitation energy exceeds 8a it is unlikely that a complex fragment could be produced since the excitation energy would exceed the binding energy per nucleon. A limiting temperature of 8 MeV then follows from the equation $8a = \frac{a}{8}T^2$. (No such limit is required in the production of nucleons from the participant fireball region). In this spirit the saturation of the spectator curve could be described as the "boiling point of nuclear matter", in analogy with the higher temperature saturation for hadronic matter.[29,79] These aspects would require further discussion which we shall not attempt here.

The saturation is interpreted as the rapid onset of abrasion at 20 MeV/nucleon, and according to the picture of the heavy ion collision in Figs. 1.3 and 1.4 there must be a simultaneous onset of fireball production. On the participant curve the transition from a localised hot-spot, trapped between the adjacent nuclei, and a separated fireball should also occur around 20 MeV/nucleon, when the temperature of the excited region is 8 MeV. On a (continued) naive basis, this transition is expected at a collision speed close to the velocity of sound,[28] if the initial excitation is carried by coherent, collective compressional modes. The relaxation time for the spreading of this energy over the nuclei is related to the frequency of the modes, which in turn depends on the speed of sound in nuclear matter. At higher collision velocities, the production of a localised region of excitation between the separating nuclei could be created. For a value of the compressibility constant K between 200 and 300 MeV, the associated value of $v_s = (K/9m)^{\frac{1}{2}}$ ranges from 0.15c to 0.19c, just in the region of the observed onset of the participant-spectator description.[28]

This description of the evolution of heavy ion collisions is based on rather global and macroscopic considerations. A detailed understanding of the transitions in Fig. 1.6 must ultimately come from a microscopically based theory. Indeed there has been some progress towards this goal for the spectator components by means of direct reaction theories of projectile fragmentation,[30,31] two-body transfer reactions,[32,33] surprisal analysis,[34] and incomplete fusion.[35] All of these approaches[36] infer a transitional behaviour in the region of 15 MeV/nucleon. It has also been shown[37] using perturbation theory that the transition probability for a heavy ion reaction leads to an expansion for the cross section in terms of y, the ratio between the duration of a nucleon-nucleon collision and the elapsed time between two successive interactions. There is a Markovian part independent of y and a non-Markovian part containing an explicit y-dependence. This decomposition also shows that a transition from Markovian behaviour occurs around 20 MeV/nucleon. Nevertheless we believe that our approach carries some merit in delineating the broad features of peripheral and central collisions over a large energy region.

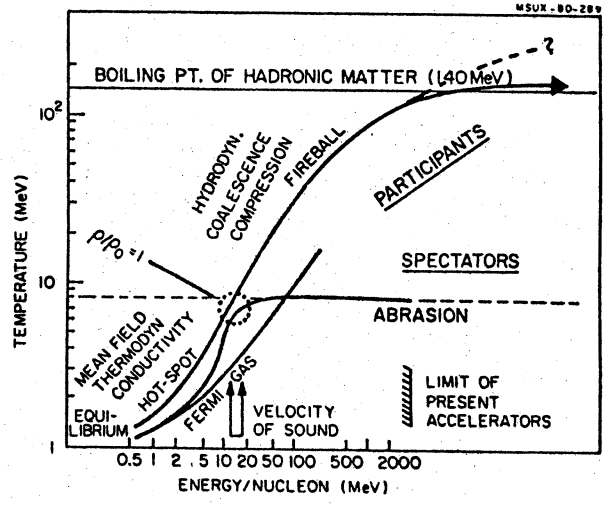

FIG. 1.10

We look on the evolution as proceeding along three characteristic paths with a branch point at 20 MeV/nucleon. Along these paths various interesting aspects of the physics of nucleus-nucleus collisions can be explored, as illustrated in Fig. 1.10. The low energy path bifurcates into the participant and the spectator paths. At low energies complete statistical equilibrium is frequently attained as described by the Fermi gas equation of state.[38] Higher temperatures are generated by restricting the degrees of freedom, for example in a hot-spot. Then information on the temperature dependence of the mean free path, thermal conductivity and viscosity might be deduced.[39] Beyond the branch point, higher temperature nuclear matter is formed and the hot-spot evolves into a fireball, while the Fermi gas becomes more and more like a classical gas. Here the mean free path may become very short[39] and the mean field description, which is successful for much of the low energy region, may be replaced by nuclear hydrodynamics.[40-43] The branch point at around 15 MeV/nucleon may also permit the observation of hot-spots formed at greater than normal nuclear density[44] as the nuclear matter becomes compressed in the nascent fireball. The formation of more complex clusters may also change character across this region, in going from thermodynamic emission at low energies to coalesence[45] in the fireball at high energies. Along the spectator path for the heavy fragments there must be an evolution from the production of deeply-inelastic projectile and target fragments at low energies[46] to the rapid abrasion of the cold spectators at high energies.

Some of these aspects are explored in the subsequent two lectures. For it is clear that these paths are not preexisting in the complex forest of heavy ion collisions. We have only rough signposts and the paths must be forged in the face of "harsh, stubborn and irreducible facts". Also it will finally be in deviations from the simple paths that the most interesting aspects of the collisions may be found. The appearance of a phase transition, for example, to a new state of nuclear matter at high density could perturb the smooth trend of the temperature[7,43] with energy, as the condensation energy is released. Even along the simpler spectator path, interesting effects may be observed. For example, the extent of ground state correlations due to deviations in real nuclei from the zero point motion of an uncorrelated Fermi gas may be accessible.[26] In the next lectures we deal with some of the foundations of the path, and in the last with some deviations from it.

2. Foundations of the Path

In this lecture we give a more detailed account of the evidence for hot-spot formation in the region of 20 MeV/nucleon. Our analysis so far indicates that a localised source could be present.[15] The existence of the hot-spot is clearly an important element in the validity of the general scheme for heavy-ion reactions in Fig. 1.10.

Just as in relativistic collisions, central events can be selected by means of a high multiplicity triggers, there is an advantage in low energy experiments to make more exclusive measurements in order to select light particles emitted in different processes. A useful trigger is given[47,48] by the set-up of Fig. 2.1. Particles are detected in a ΔE-E telescope in coincidence with fission fragments from the residual heavy target. By measuring the angle θ_{AB} between the outgoing fission fragments as well as the energies, the recoil momentum can be deduced and the momentum balance reconstructed. In Fig. 2.2, the fission coincidence spectra are shown as a function the θ_{AB} (for two different settings of the position sensitive detectors θ_A,θ_B) in an inclusive measurement (i.e. any particle detected in the forward telescope) and also for coincident protons detected over a wide range of angles (15° to 140°).

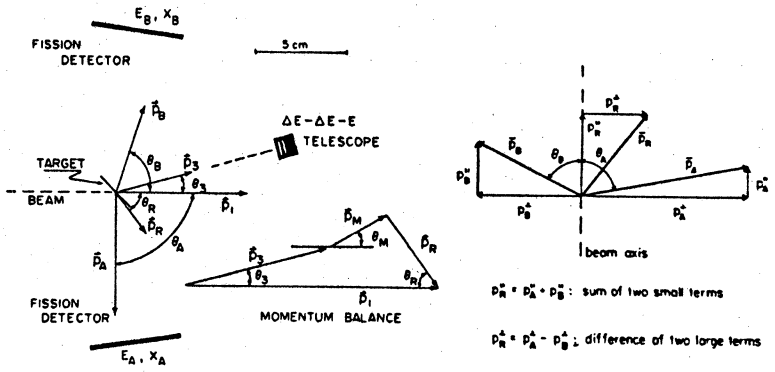

FIG. 2.1

The two peaks in the inclusive fission fragment distribution point to two dominant momentum transfers. The peak close to $\theta_{AB} = 173°$ (corresponding to the smaller transfer) is the only one appearing in coincidence with projectile like fragments (Li→O). It is therefore associated with a peripheral process, which is

known to be the main source of such particles.[24] The larger momentum transfer ($\theta_{AB} \simeq 148$) is then attributed to a more central collision. It follows that there is a sizeable probability for emission of protons in both peripheral and central collisions, but at backward angles only the central component persists. The arrows in the figure indicate the position at which the recoil momentum is equal to the difference between the mean momentum carried by the coincident light particle and the beam momentum. The agreement with the peak location suggests that the emission of only one energetic light particle is a most probable mechanism. The motion of the center of mass of any remaining light particles emitted must carry only small momentum. On the other hand, the picture of

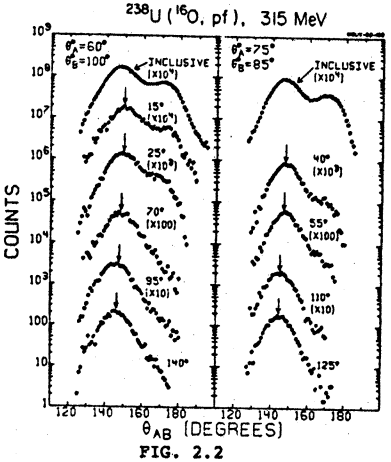

FIG. 2.2

isotropic emission from a hot source moving at half the beam velocity (as discussed in Lecture 1) is difficult to reconcile with these observations. The possibility of a hot-spot fixed on the target is however viable and it seems likely that the idea of a moving spot served as an approximate and valuable pointer to the underlying reality (at least for central collisions). In any case, the energy spectra shown in Fig. 2.3., are remarkably similar to those of the inclusive experiment (Fig. 1.7) and are fitted with an almost identical parameterization (source moving at half the beam velocity at a temperature of ≃8 MeV). It is therefore probably safe to conclude that the formal analysis of the inclusive data presented below, could also accurately be applied to the more exclusive centrally selected data.

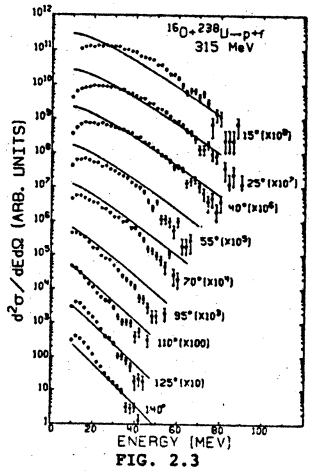

FIG. 2.3

Before proceeding to that analysis, it is worth noting that the type of coincidence experiment described can yield a wealth of information, which refines the global insights presented in Lecture 1. It is found for example, at 20 MeV/nucleon, that pure projectile fragmentation - in the spirit of the high energy abrasion limit - does not occur.[47] Rather there is a strong final state interaction with the target, but these interesting details cannot be discussed within the allotted time and space of the lectures.

The schematic model of Fig. 2.4 has been used to parameterize the hotspot formed in collisions of ^{16}O on Au at 20 MeV/nucleon.[49] Two spherical caps are chosen of equal thickness "d", which is a free parameter. For the energy of the nucleons in the hot region, a Fermi gas distribution is used without any compressional effects. The temperature is then

$$T = \left(\frac{E^*}{a}\right)^{\frac{1}{2}}$$

where E^* is the excitation eneryg and "a" is the level density parameter, $a=A_H/8$, with A_H the number of nucleons in the hot spot. For the excitation energy,

$$E^* = E_{INC} - V_c - E_{rot} .$$

Here $V_c = z_p z_T e^2/(R_p+R_T)$, the Coulomb energy of the touching configuration and $E_{rot} = L^2/2I$. The effects of the nuclear potential and of proximity friction are neglected (V_N increases the excitation, while the friction term decreases it, so the contributions cancel to some extent).

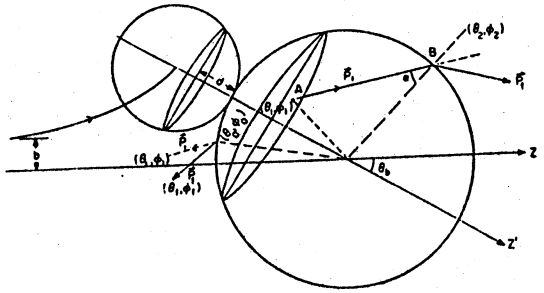

FIG. 2.4

From the boundary of the hot zone, nucleons are emitted in all directions. In the surrounding cold nuclear matter the mean free path is long and the particles reach the surface without absorption. There they undergo refraction in overcoming the nuclear potential. Nucleons emitted into the hot region are completely absorbed on account of the short mean free path in the high temperature nuclear matter. The calculated[39] variation of the mean free path with temperature is shown in Fig. 2.5. When many particles are excited out of the Fermi sea, the effect of the Pauli exclusion principle becomes less important, and two-body collisions dominate over the collisions with the wall. Thus while at temperatures of a few MeV the value of λ is commensurate with nuclear dimensions it must decrease at high temperatures, eventually approaching the values for a classical Boltzmann gas (the dashed line). Such a reduction of the mean free path is essential to the formation of a hot spot. The same idea was discussed much earlier[50] in a comparison of the time taken by an equilibrated nucleus to emit a particle, via $\tau_{sp} \simeq 0.5 \exp(13/T)$ and the relaxation time τ_R for dissipating the initial energy deposition. This increases with increasing temperature. These times are also shown in Fig. 2.5, suggesting that the condition for the observation of a hot-spot, viz $\tau_R > \tau_{sp}$ is realised at a temperature greater than 7.5 MeV. It has also been shown[51] that at incident energies below 80 MeV/nucleon, the longitudinal momentum decay length is only 1.5 fm. Thus in this energy region if a hot spot is created it should be stopped quickly, and the compressed zone might emit nucleons before the equilibration with the surrounding nuclear medium is achieved.

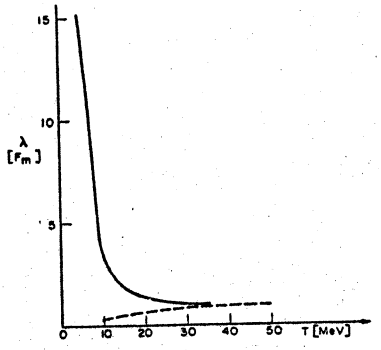

FIG. 2.5(a)

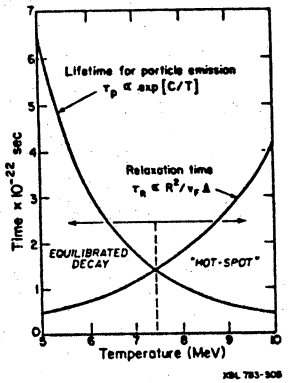

FIG. 2.5(b)

The total flux of protons $\frac{dN}{dt}$ can then be calculated at all energies $E > Vo/\cos^2\alpha$ where Vo is the depth of the single particle potential ($\simeq$ 47 MeV) and α is the angle between the incident direction and the normal to the nuclear surface (see Fig. 2.4); the energy distribution is taken from a Fermi function, and the effects of barrier penetration are included. The energy spectrum can then be deduced,

$$\frac{d\sigma}{dE} = \pi\lambda\!\!\!^{-2} \Delta t \sum_{L=0}^{L_{MAX}} (2L+1) \frac{dN}{dE}$$

in which $L_{MAX} = 110$, and Δt is the time of emission from the surface of the hot-spot. This time is adjusted to normalize the theoretical and experimental cross sections as shown in Fig. 2.6, giving a value of $t = 2\times10^{-22}$ seconds, which is of the order of, or smaller than, the collision time at 20 MeV/nucleon, viz $2R/v \simeq 4\times10^{-22}$ sec. The overall agreement with experiment is very satisfactory. Also calculated is the distribution expected for neutrons, where the peak occurs at 8 MeV, the temperature of the hot-zone. The theoretical angular distributions are also in fair agreement with the data, as illustrated in Fig. 2.7, although there is some underestimation at forward angles. It is quite possible that the forward angle data contain some contributions from other reaction mechanisms, e.g. projectile excitation and decay.[52]

The above calculations were all made for d, the depth of the spherical caps, equal to 2.5 fm. The corresponding volume of 163 fm^3 contains approximately 28 nucleons at the normal density of $\rho = 0.17$ nucleons/fm^3. The equivalent radius of a spherical volume would be 3.4 fm and it is quite intriguing (or

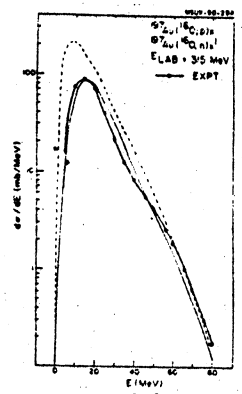

FIG. 2.6

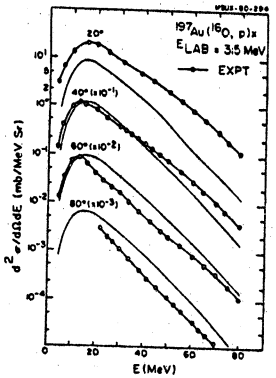

FIG. 2.7

coincidental!) that a similar volume is found for the participant region in the higher energy relativistic collisions. If this correspondance is real, it reinforces the general picture we developed in Lecture 1. Since the origins of this volume, through the coalescence model for the production of complex nuclei, represents another aspect for study over a wide energy region,[45,53] we shall present the essential physical content.

The coalescence model[54] determines the probability of condensation of nucleons, which takes place if they are within a coalescence radius p_o of each other. The probability of finding a nucleon in a sphere of momentum radius p_o, centered at p is:

$$P \quad \alpha \quad \left(\frac{4}{3}\pi p_o^3\right) \quad \frac{d^2\sigma_1(p)}{p^2 dp d\Omega}$$

where $d^2\sigma_1/p^2 dp d\Omega$ is the cross section for a single nucleon. Then the probability for finding A nucleons is just:

$$P_A \quad \alpha \quad \left(\frac{4}{3}\pi p_o^3\right)^A \left(\frac{d^2\sigma_1}{p^2 dp d\Omega}\right)^A$$

To obtain the cross section, we take the probability of finding (A-1) nucleons in the sphere p_o and multiply by 1/A times the cross section for emission of the additional particle. The final expression, with the correct constant factors is:

$$\frac{d^2\sigma_A}{p^2 dp d\Omega} = \frac{1}{A!}\left(\frac{4\pi p_o^3}{3\sigma_o}\gamma\right)^{A-1}\left(\frac{d^2\sigma_1}{p^2 dp d\Omega}\right)^A$$

where σ_o is the total reaction cross section, and γ is the relativistic correction factor. Once the cross section σ_1 for single nucleon emission is known, the cross section for any other composite fragment (d,t,^{3}He, etc.) is readily calculated.

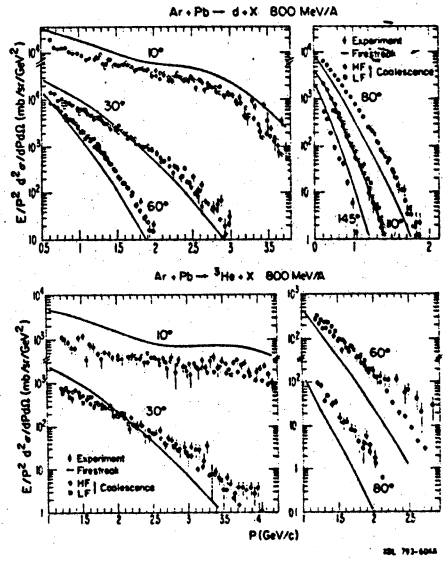

FIG. 2.8

Some typical results of this method are shown in Fig. 2.8 for the production of d and ^{3}He in Argon induced reactions at 800 Mev/nucleon.[45] The theoretical points are indistinguishable from the trend of the data (and much more successful than the firestreak model - an advanced version of the fireball). The only adjustable parameter is p_o, the coalescence radius for which a value of ≈200 MeV/c was deduced. This value derives not only for this set of data but for a wide range of projectile-target systems and incident energies.

If we now adopt a slightly different viewpoint and assume that chemical and thermal equilibrium are reached during the expansion of the fireball, it is possible to relate the value of p_o to the size of the fireball at the freeze-out density[55] essentially by phase space arguments:

$$V \alpha \frac{3h^3}{4\pi p_o^3}$$

Expressing the volume in terms of the radius of an equivalent sphere, $R=a(Ap^{1/3}+A_T^{1/3})+b$ with a=0.24 and b=1.9 fm for deuterons and 1.5 fm for t and ^{3}He, values of R 3.5-4 fm were found[45] for systems similar to ^{16}O + Pb which we have been considering at lower energies. This radius is surprisingly similar to that of the hot-spot observed at 20 MeV/nucleon. Can this be taken as further evidence for the underlying validity of the picture we presented in Lecture 1? That the evolution of the hot-spot into a fireball is observable around the collision velocity equal to that of sound. If it is a mere coincidence, we should point out that there is a third one! In an experiment to determine the size of the fireball by means of pion interferometry[56] in Argon on Pb, a value of 3.3 fm was found.

A link must also be established with the more microscopic approach of preequilibrium theory.[57,58] In such an analyses we need to know the number of excitons in the initial channel. There is a well established prescription[59] in light ion reactions: the cross section for the emission of particle β is,

$$\frac{d\sigma_\beta(E)}{dE} \alpha \quad E\,\sigma_\beta\,(E)\,U^{p+h-\beta-1}$$

where U is the excitation energy of the residual nucleus, σ_β the inverse cross section for particle β at energy E. Then a plot of

$$\log \frac{d\sigma_\beta(E)}{dE} / E\,\sigma_\beta \quad \text{vs} \log U$$

gives the slope S=p+h-β-1, where p+h is the number of particles and holes. Such a plot is shown in Fig. 2.9 for deuteron and alpha induced reactions;[60] the associated numbers for (p+h) are 4 (i.e. 3 particle - 1 hole) and 6(5 particle-1 hole) respectively. The initial excitation creates a particle-hole state, which combines with the incident nucleon. The same analysis applied to ^{16}O leads to 25, a number again remarkably close to the 28 nucleons appearing in the alternative analyses of the data with a hot-spot. Although these two representations appear quite disparate, the one dealing with the microscopic bahaviour of a nucleus with single particle wave functions, the other with macroscopic quantities like thermal conductivity and geometrical localisation, there must exist an underlying connection.[61] On account of the large initial exciton

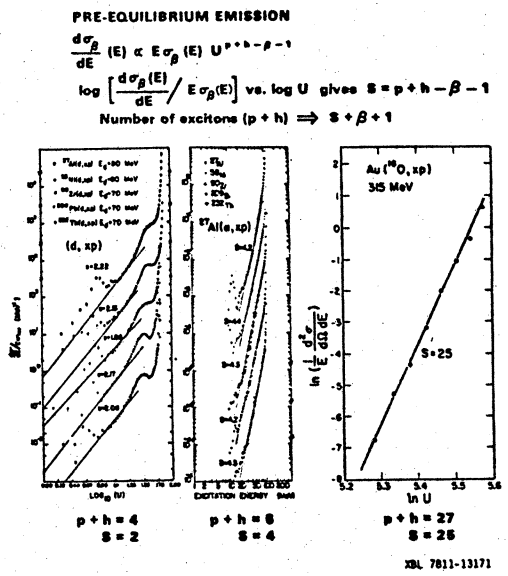

FIG. 2.9

number, it may be possible to use the concept of temperature, essential for a hot-spot description in the preequilibrium model. In light-ion reactions the situation is quite different, with small exciton numbers that change drastically with each successive nucleon-nucleon collision. Then the concept of temperature is less meaningful.

Nevertheless the hot spot model has also been used successfully to describe intermediate energy proton collisions[22] on nuclei, and even for high energy studies of hadronic matter in proton proton collisions[62] at 100 GeV/c. Here hydrodynamic concepts are invoked to describe the conductivity and transport properties of hadronic matter in the same way that they are now being applied to nuclear matter.[63,64] A unified view of light ion induced reactions is therefore already in existence. On the other hand, recent work on proton induced preequilibrium emission suggests that they may be much less complicated, and are dominated rather by single scattering.[65] In the heavy ion case, it is known, however, that single nucleon nucleon scattering does not account for the whole fireball region of rapidity space.[66-68]

The existence of hot-spots must eventually be proved through the measurement of more exclusive variables. If the scheme of Fig. 2.4 is realistic, one could look for preferential emission of high energy light particles from the side of the nucleus containing the heated zone. An asymmetry should be observed[19,69] in this emission pattern relative to the direction of the residual nucleus, since in some directions there is shadowing by the spectator nucleus. For the experiments with ^{16}O on Au discussed in this lecture, the effect has been searched for, by measuring the correlation pattern of high energy particles in coincidence with the residual ^{12}C fragment from the projectile.[70,71]

From a measurement of cross sections, energies and angles one can deduce $d^3\sigma/dE_{12}d\Omega_{12}d\Omega_{3-12}$ in the rest frame of the projectile, as a function of E_{12} the energy available in the system 12 comprising the α and ^{12}C. (The notation 3-12 refers to particle 3 relative to the center of mass of 12). The black dots in Fig. 2.10 show the spectra for the case of ^{12}C detected at 17° and the α particle at 9°, on the right hand figure and at 25° on the left hand side. These correspond to α emission towards and away from the beam direction. Each spectrum has two peaks, for emission in the forward and backward directions, and there is a pronounced minimum at E_{12}=0. This could arise from the Coulomb repulsion between the α-particle and projectile residue. Also the cross section in the forward and backward directions are of comparable magnitude. This symmetry would be expected even in the case of a hot-spot.

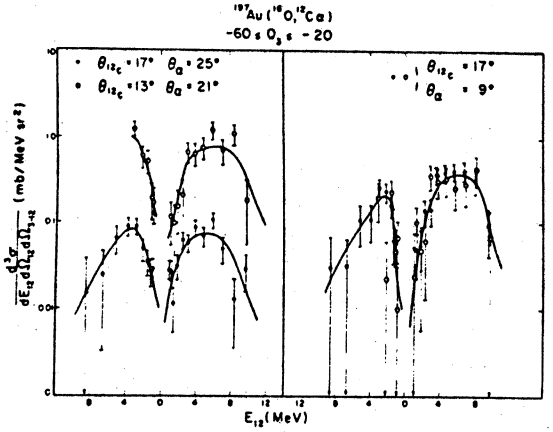

FIG. 2.10

More important is the question of the left-right asymmetry which bears on the question of the contact zone on the side of the projectile facing the target. Although such an asymmetry (roughly a factor of 5) is indeed observed with the higher value on the side correspoinding to a hot-spot formation, it is not possible to attribute the effect to this source unambiguously. Since the heavy-ion fragment is detected at a fixed angle, the direction of the decaying nucleus, in this case $^{16}O^*$, must change, and the change in the primary angular distribution could well account for the asymmetry in Fig. 2.10 of approximately a factor of 5. In an attempt to keep the primary direction approximately constant, a comparison with a measurement for carbon detected at 13° and the α at 21° is also shown (open points at left; the open points on the right are merely a repeat of the θ_c=17°, θ_α=9° configuration). The estimated range of primary angles in the laboratory is estimated to be (15.7° - 16.9°) for the right hand side and (15.9° - 17.1°) for the left. The asymmetry is now removed and even reversed. In order to reveal the effect of asymmetries due to more exotic reaction mechanisms, a very careful set of measurements and theoretical predictions are required - neither of which exist. In the case of hot-spot emission from a heavy nucleus, however, the above complications are less troublesome, and such an experiment and analysis has been done at lower energies[19,63] as mentioned in Lecture 1.

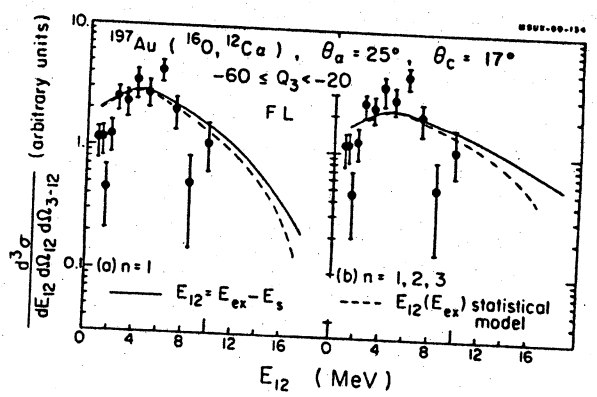

FIG. 2.11

As an example of a first step towards a more precise comparison, we describe a calculation based on the abrasion model.[72] The application of this model at 20 MeV/nucleon is consistent with the view of heavy-ion reactions in Lecture 1, in which this energy region heralds the onset of the participant-spectator description. The first abrasion stage of the reaction is calculated with the

Glauber model in which a few surface nucleons in the overlap volume scatter and exchange angular momentum at the energy of 20 MeV/nucleon-unlike at 2.1 GeV/nucleon - the nucleons are not free to leave the prefragment, but deposit all their energy and angular momentum in the prefragments which subsequently thermalise and decay statistically. (In a hot spot description this second stage of the reaction would require different treatment). The calculated excitation spectrum for $^{16}O^*$ can be converted into an E_{12} spectrum for $^{12}C+\alpha$ coincidences. The spectra shown in Fig. 2.11 correspond to the excitations for one and up to three knocked on nucleons. The solid curves were obtained by assuming that all states above threshold decay to the ground state of ^{12}C; the dashed curves are the result of a complete statistical model calculation. For comparison we show the experimental E_{12} spectrum, for a case where the total reaction Q value, Q_3, lies between -20 and -60 MeV. (This choice is approximate, since both projectile and target should be excited according to the theory). The basic features of the data are reproduced, and it remains for future work to establish whether the deviations will come from refinements in the treatment of the second stage, e.g. in localisation of the excitation rather than the assumed complete statistical equilibrium.

Here we leave the discussion of the formation and decay of hot-zones in heavy-ion collisions. One can fairly sum up the content of both the lecture and the hot-spots by a paraphrase of Churchill's words, "Never was so much contained in so little in such a short time". In the next lecture we discuss some signs of radical deviations from the unification scheme we presented in the first lecture, and which we attempted to justify in the second.

3. Deviations from the Path

The first deviations from the "unification scheme" of Figs. 1.6 and 1.10 which we shall discuss occur along the spectator path, at an incident energy in the region of 100 MeV/nnucleon.[73] We recall from Lecture 1, that the spectator model predicts a momentum dispersion of the fragments which is determined by the Fermi momentum distribution for both the components parallel and perpendicular to the beam directions. In the projectile frame, the distribution is of the form:

$$P(p) \propto \exp - \left[\frac{P_{11}^2}{2\sigma_{11}^2} + \frac{P_\perp^2}{2\sigma_\perp^2} \right]$$

In the first lecture we showed that q_{11}^2 is well discribed at many energies by the expression $\sigma_o^2 \frac{F(A-F)}{A-1}$ where σ_o^2 is related to Fermi momentum $p_F^2/5$ and F, A are the mass numbers of fragment and projectile. At high energies it is also found from a measurement of the angular distributions that $\sigma_{11}=\sigma_\perp$ within 10%. At 100 MeV/nucleon, this equality breaks down.

Fig. 3.1 shows values of $\sigma_\perp$ deduced from angular distributions of ^{16}O on Al and Au at energies of 92.5 and 117.5 MeV/nucleon.[73] In all cases the $\sigma_\perp$ values are much larger than predicted by the expression $\sigma_o^2 \frac{F(A-F)}{A-1}$, which is shown by

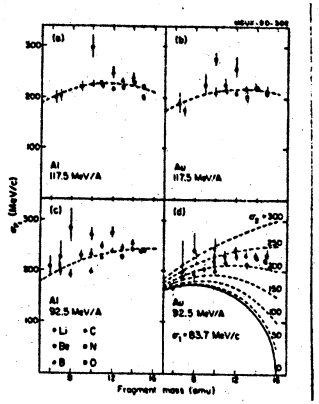

FIG. 3.1

the solid curve labelled $\sigma_2=0$ in section (d) of the figure. It appears that more sideways momentum transfer is imparted to the projectile. To see how this momentum modifies our earlier expressions we proceed as in the first lecture:

$$\langle P_F^2 \rangle = F\langle p^2 \rangle + F(F-1)\langle Pi \cdot Pj \rangle \quad .$$

But now we must also write,

$$\langle P_A^2 \rangle = A\langle P^2 \rangle + A(A-1)\langle pi \cdot pj \rangle$$

and

$$3\sigma_F^2 = \langle (P_F - \langle P_F \rangle)^2 \rangle$$

$$= \langle P_F^2 \rangle - \langle P_F \rangle^2$$

where

$$\langle P_F \rangle = \frac{F}{A} \langle P_A \rangle$$

The main difference compared to the previous derivation is that $\langle P_A \rangle$ is no longer zero. We obtain finally, by collecting terms,

$$\sigma_P^2 = \frac{F(A-F)}{A-1}\,\sigma_o^2 + \frac{F(F-1)}{A(A-1)}\,\sigma_1^2$$

where $\sigma_1^2 = \frac{1}{3}\langle (P_A - \langle P_A \rangle)^2 \rangle$ | or $\frac{1}{2}\langle P_{A|}^2 \rangle$, the variance of the transverse momentum of the projectile at the time of fragmentation. The quality of the fit to the experimental $\sigma_\perp^2$ values is shown in Fig. 3.1, for values of $\sigma_o \approx 86$ MeV/c (as before) and $\sigma_1 \approx 230$ MeV/c. The effect of varying σ_1 is shown in panel (c), in which for $\sigma_1 = 0$ the original parabolic mass dependence is retrieved.

The expected values of σ_2 have been calculated from the classical deflection function of the projectile in the nuclear and Coulomb potential.[73] The range of impact parameters is determined from the observed ratio of the fragmentation cross section to the total, $\sigma_F/\sigma_T \approx 0.6$. Then $\sigma_1^2 = \frac{1}{2} P_A^2 \int N(b) \sin^2 \theta(b)\,db$, where $N(b) = 2b/(R^2-b^2)$ is the weighting factor for impact parameter. For a potential of Saxon-Woods form ≈ 70 MeV deep, the calculated values of σ_1 are 170-200 MeV/c which are of the correct order. A satisfactory fit to the differential cross section is also obtained. It must be noted, however, that there are systematic departures in the variation of $\sigma_\perp$ with isotope that are not reproduced by the formalism derived here (see Fig. 3.1).

Perhaps it is necessary to incorporate other potentials to fully account for the sideways deflections. At this energy, for example, there may be compresional effects, as suggested in hydrodynamical calculations.[74] An example for ^{20}Ne on U at 400 MeV/nucleon is shown in Fig. 3.2, in which the compressional bounce-off is evident as a function of time in units of 10^{-23} sec for all three impact parameters. We have also seen in the last lecture that at 100 MeV/nucleon the

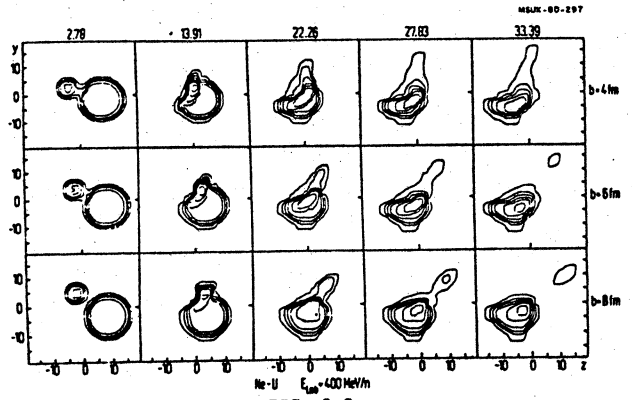

FIG. 3.2

mean free path becomes very short as required in hydrodynamics, but this energy is not so high that the nucleus may have lost all cohesiveness. It is therefore interesting to make an estimate of the magnitude of momentum transfer expected from compression.[75]

The momentum transfer is given by

$$\Delta p_\perp = -\int_{-\infty}^{\infty} F(t)\,dt$$

where F is the compressional force; F=PS with P the internal pressure and S the exposed surface area. For the pressure we write

$$P(\rho) = \rho^2 \frac{\partial E_c}{\partial \rho} = \frac{K}{18\rho_o}\,(\rho^2 - \rho_o^2)$$

in which E_c is the compressional energy per nucleon and $K \approx 200$ MeV is the compression constant. The surface area exposed can be estimated from the geometrical considerations of Fig. 3.3,

$$S = \pi r^2, \quad r^2 = R_p^2 - b'^2 = R_T^2 - (b-b')^2.$$

The interaction time is approximately,

$$\Delta t = \frac{1}{v}\left[(R_T+R_p)^2 - b^2\right]^{1/2}$$

Then

$$\Delta p_\perp = \frac{K}{18\rho_o}\,(\rho^2 - \rho_o^2)\,\frac{1}{v}\,G(b)$$

with

$$G(b) = \pi\left[R_p^2 - \left(\frac{b^2 - R_T^2 + R_p^2}{2b}\right)^2\right]\left[(R_T+R_p)^2 - b^2\right]^{1/2}$$

Guided by the ratio $\sigma_F/\sigma_T \approx 0.6$, we choose the impact parameter ≈ 8 fm, and deduce that $\Delta p_\perp \approx 250$ MeV/c can arise if $\rho \approx 1.2\,\rho_o$. A compression of this magnitude is indeed expected from full hydrodynamical calculations for ^{20}Ne + Au[76] shown in Fig. 3.4. We do not infer that such effects are observed in this experiment but merely wish to point out that the experiment is a possible way of looking for the effects of compression in peripheral collisions. The density which is reached depends critically on the equation of state, and we must devise as many means as possible of extracting information about it from the data.

Let us give another example which synthesises the above discussion with our earlier treatment of hot-spots. Recently the behaviour of a hot and compressed zone has been treated.[77] The hot zone is parameterised by the compression $\eta = \rho H/\rho_o$ and the size $\xi = R_H/R_o$ where R_o is the radius of the combined target and

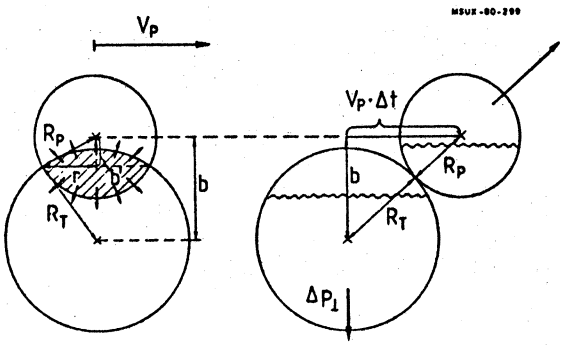

FIG. 3.3

projectile and R_H is the radius of the hot spot. The temperature is calculated with the liquid drop model, where the volume term is determined from mean field theory./78/ The effect of the temperature and density on the surface tension was also incorporated. For the system ^{16}O + Au, which we have used repeatedly in these lectures, the dependence of T on η and ξ is shown for two collision energies of 20 and 50 MeV/nucleon. One observes that for a fixed compression a smaller hot-spot will have a higher temperature. For a higher compression and for a fixed size the temperature drops, just because the available energy of relative motion must be shared between compressional energy and heat. A careful study of the temperature in the hot-spot and in the nascent fireball by the methods of Lecture 2 along the participant path of Lecture 1 might allow the extraction of ρ values. For orientation, in a hot-spot with $\xi \approx 0.5$ (commensurate with the dimensions we extracted in Lecture 2) the temperature varies from 20 to 8 MeV for compressions η=1 to 1.5. At higher energies of 50 MeV/nucleon, the differences are less marked. It may turn out therefore, that the detection of compression may be easiest just above the branch point at the velocity of sound in Fig. 1.10, i.e. in the region of 20 to 50 MeV/nucleon. Of course in the event of a phase transition the energy-density relationship can be radically perturbed with a concommittant change in the trend of the temperature./43/

Another observable of great interest concerns the stability of the hot zone. When the excitation energy per nucleon in an interacting volume of nucleons made up of a_1, nucleons from the projectile and a_2 from the target,

$$E^* = E_{LAB} \frac{a_1 a_2}{(a_1+a_2)^2}$$

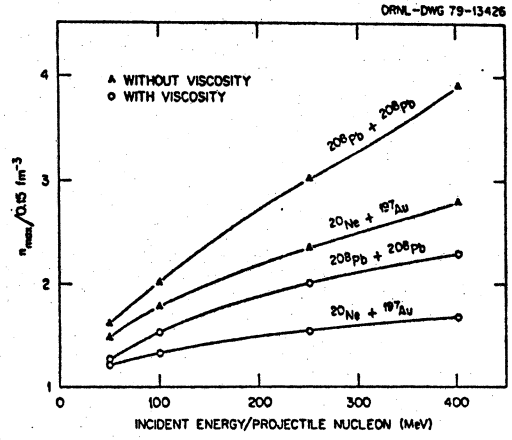

FIG. 3.4

exceeds 8 MeV, the system a_1+a_2 is unbound and will disintegrate./79/ If equal numbers from target and projectile participate $a_1=a_2$ and E_{LAB} = 32 MeV/nucleon. A more refined calculation, with a proper treatment of surface and volume affects, places the explosion between 30 and 50 MeV/nucleon, corresponding to temperatures in the hot-spot (see Fig. 3.5) of 18 to 23 MeV (ignoring compression)./77/

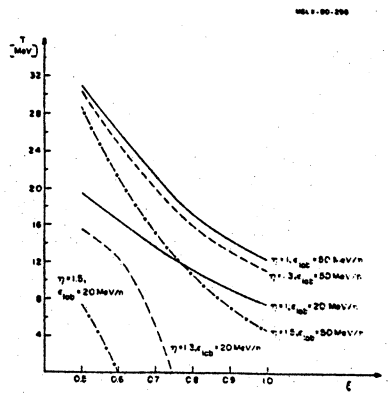

FIG. 3.5

Experimentally such explosions are observed, like the dramatic example/79/ for ^{12}C in an emulsion at 91 MeV/nucleon shown in Fig. 3.6(a). When the pro-

bability of such explosions (of the projectile or a part of the combined system comparable in size to the projectile) is investigated as a function of energy, the curve shown in Fig. 3.6(b) results.[80,81] There appears a rapid increase up to 200 MeV/nucleon followed by a levelling off at higher energies. This type of study could also be used to determine the densities and temperatures of the exploding hot-spot or fireball as a function of energy over the critical region from 20 MeV/nucleon to, say, 100 MeV/nucleon. The results can be compared with the theoretical predictions for equations of state, such as that shown in Fig. 3.7(a), which shows[77] that the binding energy would become zero at a

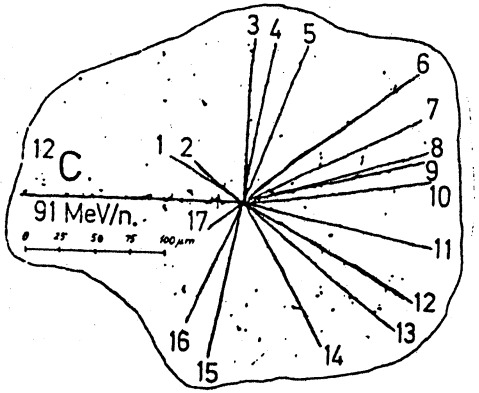

FIG. 3.6(a)

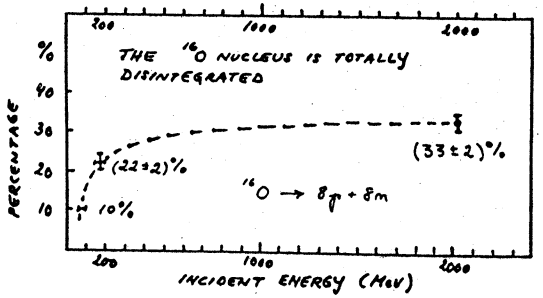

FIG. 3.6(b)

compression of 1.3 and a temperature of 23 MeV. The complete disintegration can also be studied through the action of the mean field. It is found that in the overlapping region of the two nuclei the rapid increase in the density leads to a positive increase in the mean field potential.[40/76] The appearance of this

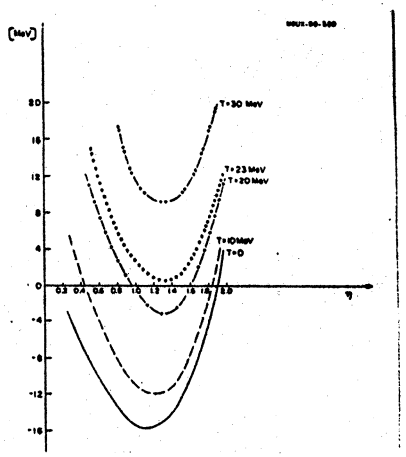

FIG. 3.7(a)

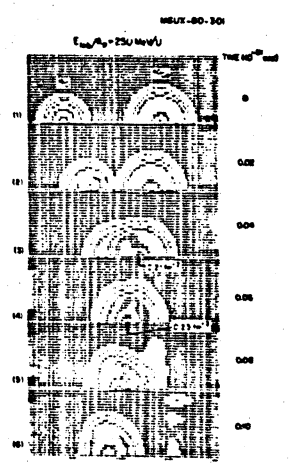

FIG. 3.7(b)

repulsive potential-the volcano effect-causes some of the nucleons to become unbound. This effect in turn lowers the depth of the self-consistent potential and leads to disintegration of one of the two nuclei. In Fig. 3.7(b) the disintegration of ^{16}O in a collision with ^{40}Ca at 250 MeV/nucleon is observed in a series of time frames. The detailed study of this effect with energy may be sensitive to the predictions of different equations of state.

It appears that intermediate energy heavy-ion collisions offer many opportunities for the study of new phenomena. According to the general scheme we have presented in the lectures, researches into these new aspects can begin at 20 MeV/nucleon. Whether this intermediate region from 20 to 200 MeV/nucleon will reveal truly exotic phenomena remains to be seen. The phase diagram shown in Fig. 3.8 indicates the regions in temperature and density space at which transitions to new forms of matter might occur.[1] Phase transitions are delicate things and the right combination of circumstances must be provided. History has shown that given that chance, they will usually occur. To produce pion condensates and density isomers high densities are called for, but at the same time the temperature must be kept low.[82,83] Very high energy collisions tend to produce high temperatures as indicated by the two trajectories calculated in a cascade model for the values of ρ and T as a function of time.[84] The lower energy of 1.7 GeV/nucleon probes the highest density. At still lower energies

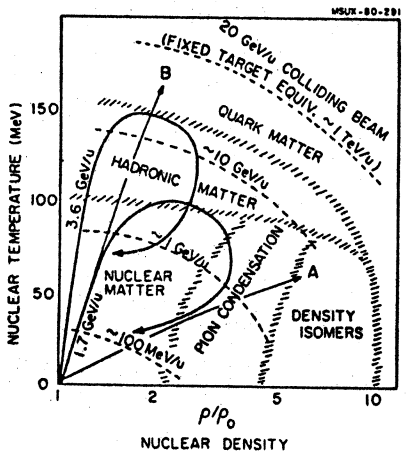

FIG. 3.8

one can speculate that higher densities are achieved with even lower temperatures, together with any anomalies according to the framework discussed in this lecture.

There are indications at higher energies for anomalies, such as illustrated in Fig. 3.9. The specific entropy of the nuclear fireball can be deduced from the asymptotic ratio of deuteron to proton creation.[6] More entropy appears to be generated during the collision that is predicted from even soft equations of state. The paper concludes, "It could be that there are strong attractive forces present in the hot dense nuclear medium, thus raising the entropy. It could also be that many more mesonic and baryonic particulate degrees of freedom are excited at this energy than expected. Or it could be that collective degrees of freedom, such as due to pion condensation are the culprits. Or perhaps the nucleons dissociate into quarks." In order to clarify the origins of the discrepancy, it is clear that we need excitation functions measured over a broad region in small steps. In that way deviations will become convincing regardless of the overall scale of comparison between experiment and theory. The message behind these lectures is that these excitation functions, along with their motivating ideas, "the message and the medium", can be carried down to much lower energy regions than hitherto expected, and where there should be no contradictions between experiment and theory. In the framework of the unification scheme in Fig. 1.10

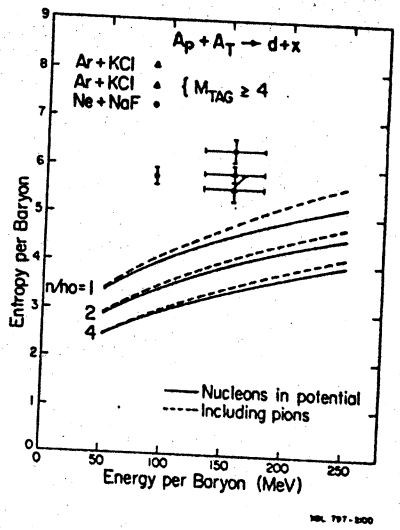

FIG. 3.9

the branch point at around 20 MeV/nucleon becomes a launching point for the exploration of new paths in heavy ion collisions. At the moment we do not know for sure where these paths will lead, but we can be sure that, in Capra's words,[85] they are good paths - paths with a heart - and they must be followed. Even if they do not lead to exotic discoveries, we can be confident that there will be sufficient returns to make the enterprise worthwhile. Along the simpler, and more well trodden, spectator path of Fig. 1.10, we already know that intermediate energy collisions allow us to study exotic nuclei very far removed from the valley of stability[86] and possibly through the rapid snapshot of the abrasion process to observe the zero point motion of nuclei, modified by the many correlations that may be present in ground state of a nucleus.[26]

ACKNOWLEDGEMENTS

The author is indebted to C.K. Gelbke, D. Sperber and H. Stocker for providing results prior to publication. It is also a pleasure to acknowledge informative discussions with P.J. Siemens.

This material is based upon work supported by the National Science Foundation under Grant No. Phy 78-22696.

References

1. The Venus project, PUB-5075, Lawrence Berkeley Laboratory, 1979.

2. H. Stöcker, J.A. Maruhn and W. Greiner, Phys. Rev. Lett. 44, 725 (1980).

3. R. Stock, H.H. Gutbrod, W.G. Meyer, A.M. Poskanzer, A. Sandoval, J. Gosset, Ch. King, G. King, Ch. Lukner, N. Vansen, G.D. Westfall and K. Wolf. Phys. Rev. Lett. 44, 1243 (1980).

4. P.J. Siemens and J.O. Rasmussen, Phys. Rev. Lett. 42, 880 (1979).

5. H. Stöcker, J. Hofmann, J.A. Maruhn and W. Greiner, Lectures at Erice School on Heavy Ion Interactions at High Energies (1979).

6. P.J. Siemens and J.I. Kapusta, Phys. Rev. Lett. 43, 1486 (1979).

7. H. Stöcker, A.A. Ogloblin, W. Greiner, G.S.I. - Preprint 79-19 (1979).

8. W.J. Romo and P.J.S. Watson, Phys. Lett. 88B, 354 (1979).

9. J.D. Bjorken and L.D. McLerran, Proc. of Conf. on Cosmic Rays and Particle Physics, ed. T.K. Gaisser, p. 317 (1978).

10. K. Van Bibber, W. Pang, M. Avery and E. Bloemhof, LBL Preprint - 9979.

11. S. Nagamiya and D.J. Morissey, LBL Preprint 10461, submitted to Phys. Lett. B.

12. W.G. Meyer, H.H. Gutbrod, Ch. Lukner and A. Sandoval, Phys. Rev. C., to be published.

13. P.J. Siemens and J.O. Rasmussen, Phys. Rev. Lett. 42, 880 (1979).

14. K.K. Glendenning and Y.J. Karant LBL Report 8653 and to be published in Nucl. Phys. A.

15. T.J.M. Symons, P. Doll, M. Bini, D.L. Hendrie, J. Mahoney, G. Mantzouraris, D.K. Scott, K. Van Bibber, Y.P. Viyogi, H.H. Wieman and C.K. Gelbke, Phys. Lett. B, to be published.

16. S. Nagamiya, Nucl. Phys. A335, 517 (1980).

17. H. Homeyer, C. Egelhaaf, H. Fuchs, A. Gamp, H.G. Bohlen and H. Kluge, Proc. of Symp. on Heavy Ion Physics from 10 to 200 MeV/nucleon, BNL 51115, 769 (1979).

18. L. Westerberg, D.G. Sarantites, D.G. Hensley, R.A. Dayras, M.L. Halbert, J.H. Barker, Phys. Rev. C18, 797 (1978).

19. H. Ho, R. Albrecht, W. Dünnweber, G. Graw, S.G. Steadman, J.P. Wurm, D. Disdier, V. Rauch and F. Schiebling, Z. Phys. A283, 235 (1977).

20. H. Utsunomiya, T. Nomura, T. Inamura, T. Sugitate and T. Motobayashi, Nucl. Phys. A334, 127 (1980).

21. H. Löhner, B. Ludewigt, D. Frekers, G. Gaul and R. Santo, Z. Phys. A292, 35 (1979).

22. N. Stelte, M. Westrom and R. M. Weiner, Preprint 1980.

23. J.R. Wu, C.C. Chang and H.D. Holmgren, Phys. Rev. C19, 659 and 698 (1979)

24. C.K. Gelbke, C. Olmer, M. Buenerd, D.L. Hendrie, J. Mahoney, M.C. Mermaz and D.K. Scott, Phys. Rep. 42, 312 (1978).

25. A.S. Goldhaber, Phys. Lett. 53B, 306 (1974).

26. Y.P. Viyogi, T.J.M. Symons, P. Doll, D.E. Greiner, H.H. Heckman, D.L. Hendrie, P.J. Lindstrom, D.K. Scott, K. Van Bibber, G.D. Westfall, H.H. Wieman, H.J. Crawford, C. McParland and C.K. Gelbke, Phys. Rev. Lett. 42, 33 (1979).

27. E.J. Moniz, I. Sick, R.R. Whitney, J.R. Ficenec, R.D. Kephart and W.P. Trower, Phys. Rev. Lett. 26, 445 (1971).

28. D.K. Scott, M. Bini, P. Doll, C.K. Gelbke, D.L. Hendrie, J.L. Laville, J. Mahoney, A. Menchaca-Rocha, M.C. Mermaz, C. Olmer, T.J.M. Symons, Y.P. Viyogi, K. Van Bibber, H.H. Wieman and P.J. Siemens, LBL Preprint 7729.

29. D.K. Scott, Proceedings of the 1st Oaxtepec Conference, Instituto de Fisica, Vol. 1, 221 (1978).

30. K.W. McVoy and C. Nemes, Z. Phys., A295, 177 (1980).

31. R. Shyam, G. Baur, F. Rösel and D. Trautmann, Phys. Rev. C19, 1246 (1979).

32. T. Udagawa, T. Tamura, T. Shimoda, H. Frölich, M. Ishihara and K. Nagatani, Phys. Rev. C20, 1949 (1979)

33. D.F. Jackson, Phys. Lett. 71B, 57 (1977).

34. Y. Alhassid, R.D. Levine, S.G. Steadman, and J.S. Karp,
Phys. Rev. C20, 1789 (1979).

35. K. Siwek-Wilczynska, E.H. du Marchie van Voorthuysen, J. Van Popta,
R.H. Siemssen and J. Wilczynski,
Phys. Rev. Lett. 42, 1599 (1979) and ref. therein.

36. For a summary, see C.K. Gelbke,
Proceedings of the Symposium on Continuum Spectra in Heavy Ion Collisions
(San Antonio, 1979).

37. F.S. Hernandez and G. Mantzouranis,
LBL Preprint 9568 (1979), to be published in Phys. Rev. C.

38. For a discussion see W. Schroeder,
Proceedings of the Symposium on Continuum Spectra in Heavy Ion Collisions,
San Antonio, 1979.

39. S.I.A. Garpman, D. Sperber and M. Zielinska-Pfabe,
Preprint 1980.

40. C.Y. Wong,
Symposium on Heavy Ion Physics from 10 to 200 MeV/nucleon, Brookhaven
National Laboratory, BNL - 51115, 379 (1979).

41. A.R. Bodmer and C.N. Panos,
Phys. Rev. C15, 1342 (1977) ;
A.R. Bodmer,
Proceedings of Conference on Theoretical Aspects of Heavy Ion Collisions,
ORNL Report 770602.

42. P. Bonche, S. Koonin and J.W. Negele,
Phys. Rev. C13, 1226 (1976).

43. H. Stöcker, R.Y. Cusson, J.A. Maruhn and W. Greiner,
Z. Phys. A294, 125 (1980).

44. S.I.A. Garpman, D. Sperber and M. Zielinska-Pfabe,
Phys. Lett. 90B, 53 (1980)

45. M. C. Lemaire, S. Nagamiya, S. Schnetzer, H. Steiner and I. Tanihata,
Phys. Lett. 85B, 38 (1979).

46. A. Olmi, U. Lynen, J.B. Natowitz, M. Dakowski, P. Doll, A. Gobbi, H. Sann
H. Stelzer, R. Bock and D. Pelte,
Phys. Rev. Lett. 44, 383 (1980)

47. P. Dyer, T.C. Awes, C.K. Gelbke, B.B. Back, A Mignerey, K.L. Wolf,
H. Breuer, V.E. Viola Jr., and W.G. Meyer,
Phys. Rev. Lett. 42, 560 (1979).

48. T.C. Awes, C.K. Gelbke, B.B. Back, A.C. Mignerey, K.L. Wolf, P. Dyer,
H. Brener and V.E. Viola J.R.,
Phys. Lett. 87B, 43 (1979).

49. W.W. Morison, S.K. Samaddar, D. Sperber and M. Zielinska-Pfabe,
Preprint 1980.

50. S. Kind and G. Patergnani,
Nuovo Cimento 10, 1375 (1953)

51. M.I. Sobel, P.J. Siemens, J.P. Bondorf and H.A. Bethe,
Nucl. Phys. A251, 502 (1975)

52. J.B. Ball, C.B. Fulmer, M.L. Mallory and R.L. Robinson,
Phys. Rev. Lett. 40, 1698 (1978).

53. M.C. Lemaire,
Proceedings of the Franco-Japonais Symposium, 1979.

54. H.H. Gutbrod, A. Sandoval, P.J. Johansen, A.M. Poskanzer, J. Gosset,
W.G. Meyer, G.D. Westfall and R. Stock,
Phys. Rev. Lett. 37, 667 (1976).

55. A. Mekjian,
Phys. Rev. Lett 38, 640 (1977);
Phys. Rev. C17, 1051 (1978) ;
Phys. Lett. 89B, 177 (1980).

56. S.Y. Fung, W. Gorn, G.P. Kiernan, J.J. Lu, Y.T. Oh and R.T. Poe,
Phys. Rev. Lett. 41, 1592 (1978).

57. M. Blann,
Ann. Rev. Nucl. Sci. 25, 123 (1975).

58. M. Blann, A. Mignerey and W. Scobel,
Nukleonika 21, 335 (1976).

59. J.J. Griffin,
Phys. Lett. 24B, 5 (1967).

60. J.R. Wu, C.C. Chang, H.D. Holmgren,
Phys. Rev. C19, 370 and 659 (1979).

61. R. Weiner and M. Westrom,
Phys. Rev. Lett. 34, 1523 (1975).

62. R.M. Weiner,
Phys. Rev. D13, 1363 (1976).

63. P.A. Gottschalk and M. Weström,
Nucl. Phys. A314, 232 (1979).

64. R. Weiner and M. Weström,
Nucl. Phys. A256, 282 (1977).

65. H.C. Chiang and J. Hüfner,
preprint 1980.

66. S. Nagamiya, K. Anderson, W. Brückner, O. Chamberlain, M.C. Lemaire,
S. Schnetzer, G. Schapiro, H. Steiner and I. Tanihata,
Phys. Lett. 81B, 147 (1979).

67. F.B. Yano and S.E. Koonin,
Phys. Lett. 78B, 556 (1978).

68. M. Chemtob and B. Schurmann,
Nucl. Phys. A336, 508 (1980).

69. R.M. Weiner,
Phys. Rev. Lett. 32, 630 (1974).

70. C.K. Gelbke, M. Bini, C. Olmer, D.L. Hendrie, J.L. Laville, J. Mahoney, M.C. Mermaz, D.K. Scott and H.H. Wieman,
Phys. Lett. 71B, 83 (1977).

71. M. Bini, C.K. Gelbke, D.K. Scott, T.J.M. Symons, P. Doll, D.L. Hendrie, J.L. Laville, J. Mahoney, M.C. Mermaz, C. Olmer, K. Van Bibber and H.H. Wieman,
Michigan State University, Preprint, 1980.

72. J. Hufner, C. Sanders and G. Wolschin,
Phys. Lett. 73B, 289 (1978).

73. K. Van Bibber, D.L. Hendrie, D.K. Scott, H. Wieman, L.S. Schroeder, J.V. Geaga, J.A. Cessin, R. Treuhaft, J.Y. Grossiord, J.O. Rasmussen and C.Y. Wong,
Phys. Rev. Lett. 43, 840 (1979).

74. H. Stöcker, J.A. Maruhn and W. Greiner,
Z. Phys. A293, 193 (1979).

75. H. Stöcker and B. Muller,
GSI Preprint 80-4 (1980).

76. H.H.K. Tang and C.Y Wong,
Phys. Rev. C21, 1846 (1980).

77. S.I.A Garpman, S.K. Samaddar, D. Sperber and M. Zielinska-Pfabe,
Preprint 1980.

78. J.D. Walecka,
Phys. Lett. 59B, 109 (1975).

79. J.P. Bondorf,
Proceedings of the Conference on Large Amplitude Collective Nuclear Motion, Lake Balaton, 482 (1979).

80. R. Kullberg and Oskarsson,
Z. Phys. A288, 283 (1978).

81. I. Otterlund,
Talk presented at Symposium on Intermediate Energy Heavy Ion Collisions, Copenhagen, 1979.

82. V. Ruck, M. Gyulassy and W. Greiner,
Z. Phys. A277, 391 (1976).

83. M. Gyulassy and W. Greiner,
Ann. Phys. 109, 485 (1977).

84. V.D. Toneev,
Private communication 1980.

85. F. Capra, The Tao of Physics.

86. T.J.M. Symons, Y.P. Viyogi, G.M. Westfall, P. Doll, D.E. Greiner, H. Faraggi, P.J. Lindstrom, D.K. Scott, H.J. Crawford and C. McParland,
Phys. Rev. Lett. 42, 40 (1979).

87. G.D. Westfall, T.J.M. Symons, D.E. Greiner, H.H. Heckman, P.J. Lindstrom, J. Mahoney, A.C. Shotter, D.K. Scott, H.J. Crawford, C. McParland, T.C. Awes, C.K. Gelbke and J.M. Kidd.
Phys. Rev. Lett. 43, 1859 (1979).